COMPARISON AMONG VARIOUS NUMERICAL MODELS DESIGNED FOR COMPUTING INFRARED COOLING

HUGH M. STONE and SYUKURO MANABE
Geophysical Fluid Dynamics Laboratory, ESSA, Princeton, N.J.

ABSTRACT

The scheme of computing the temperature change due to long wave radiation, developed by Manabe and Strickler and incorporated into the general circulation models developed at the Geophysical Fluid Dynamics Laboratory of ESSA, is compared with a group of other numerical schemes for computing radiative temperature change (e.g., the scheme of Rodgers and Walshaw). It is concluded that the GFDL radiation model has the accuracy comparable with other numerical models despite various assumptions adopted.

1. INTRODUCTION

Recently, Rodgers and Walshaw [20] proposed an improved method of computing the distribution of infrared cooling in the atmosphere. The major characteristics of their method as compared with the approach of radiation charts [4, 17, 25] are the subdivision of water vapor bands into many intervals and the use of a random model in representing the absorptivity curves.

The radiation model described by Manabe and Strickler [12] and Manabe and Wetherald [14] has been used at the Geophysical Fluid Dynamics Laboratory (GFDL) for the numerical studies of general circulation and the thermal equilibrium of the atmosphere during the past several years (see Smagorinsky et al. [22], Manabe et al. [13], Manabe and Hunt [15], and Hunt and Manabe [7] in addition to the papers cited above). Their method is essentially an adaptation of the traditional method of the radiation chart (i.e., Yamamoto [25], Elsasser [4], and Möller [17] chart) to the numerical method of computing radiative flux. Therefore, it is worthwhile to compare among the results which are obtained from these two schemes as well as some other numerical schemes (i.e., Plass [18, 19], and Hitchfeld and Houghton [5]). The model of Rodgers and Walshaw [20] has been programmed at GFDL in order to construct a general circulation model involving the upper atmosphere as well as the lower atmosphere. It was therefore possible to compare the performance of this model with those of other models.

2. CHARACTERISTICS OF THE MODELS

For the sake of simplicity, the following abbreviated symbols are used to identify various models:

(R-W) model—Rodgers and Walshaw [20];

(M-S) model*—Manabe and Strickler [12], Manabe and Wetherald [14];

(Plass) CO_2 model—Plass [19];

(Plass) O_3 model—Plass [18];

(H-H) O_3 model—Hitchfeld and Houghton [5];

(K) model—Kaplan [9].

(R-W) MODEL

The (R-W) model subdivides the 6.3-micron band, the rotation band, and the continuum of water vapor into 19 subintervals. Two of these subintervals contain the 15-micron carbon dioxide band and the 9.6-micron ozone absorption band. The transmissions of the two gases are multiplied together in these overlapping bands. A random model is used to represent the absorptivity for each subinterval. The Curtis-Godson approximation is used to estimate the effective pressure for absorption.

The random model fits very well the absorption band of water vapor. However, it fits poorly the 15-micron band of carbon dioxide. In figure 1a, solid lines show the absorptivity obtained by Burch et al. [2] from laboratory experiment. Dashed lines show the computed absorptivity based upon the random model. The mean line intensity and the mean half width, adopted for this computation, are determined theoretically (see table 6 of [20]). This figure shows that the agreement between the computed curves and the experimental curves is very poor. They coincide with each other only when pressure is low and accordingly, the degree of overlapping between the lines is small. The random model also fits very badly the ozone absorptivity, as shown by figure 1b. In this case the random model parameters were determined

*Improved version of the model constructed by Manabe and Möller [11].

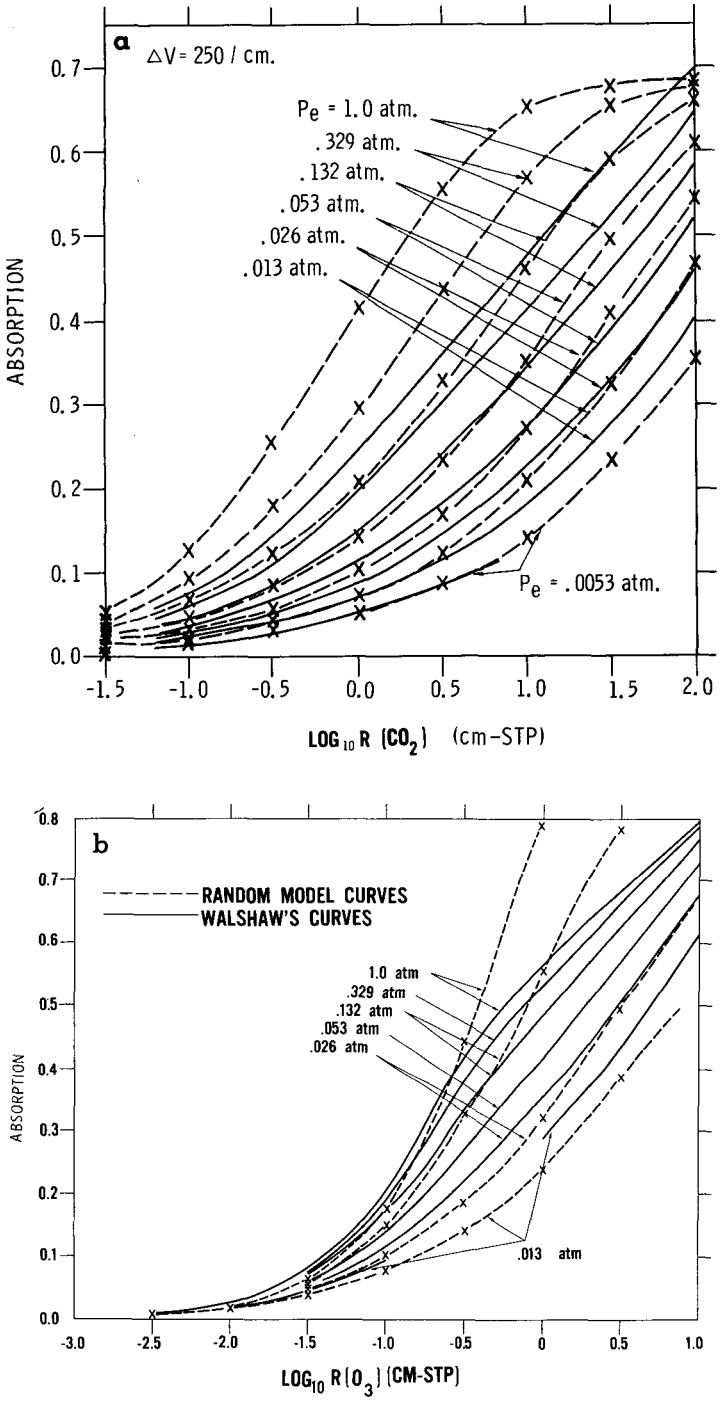

FIGURE 1.—(a) Carbon dioxide absorption. Solid curves observed by Burch et al. [2], dashed curves computed by random model. (b) Ozone absorption. Solid curves observed by Walshaw [24], dashed curves computed by random model.

empirically using the least squares curve-fitting method of Rodgers and Walshaw [20] and the laboratory data of Walshaw [24]. In view of this poor agreement for both carbon dioxide and ozone, we programmed the following two versions of the (R-W) model:

$(R\text{-}W)_1$ Model: This model uses the random model absorptivity. The effect of the temperature dependence of line intensity is incorporated in the model as suggested by [20].

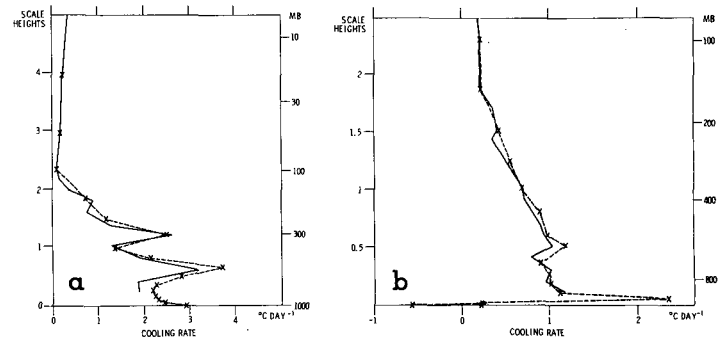

FIGURE 2.—Water vapor cooling rate of original Rodgers and Walshaw [20] model, solid lines, compared to GFDL version of (R-W) model, dashed lines: (a) tropical atmosphere; (b) Arctic atmosphere.

$(R\text{-}W)_2$ Model: Carbon dioxide absorptivity, which is measured by Burch et al. [2] under various pressures, is used for this model. The temperature dependence of this absorptivity is determined from the theoretical computation of Sasamori [21]. The ozone absorptivity determined by Walshaw [24] is used with no correction for temperature.

Both versions of the model described above differ slightly from the original model of Rodgers and Walshaw. Their original model computed cooling rates by means of a flux divergence equation, while our version does this computation by taking flux differences across each layer. The water vapor spectrum is divided slightly differently and the vertical spacing of levels is different in our versions of the model.

Our $(R\text{-}W)_1$ model was compared with the original (R-W) model for the case of cooling due to water vapor in a tropical atmosphere and an Arctic atmosphere. The results are shown in figures 2a and 2b, respectively, which correspond to figures 11d and 11e of [20]. The results are similar.

The computation time for an 18-level (R-W) model is about 1.5 sec. on the UNIVAC 1108 computer.

Earlier, a method very similar to the (R-W) model was proposed by McClatchey [16] for the computation of infrared cooling due to water vapor. There are minor differences between the two. For the rotation band of water vapor, McClatchey uses an empirically determined general transmission function instead of the random model transmission function. McClatchey's water vapor rotation band (50–680 $cm.^{-1}$) does not coincide with the (R-W) rotation band (0–960 $cm.^{-1}$), and McClatchey does not consider the continuum. To test the similarity of the two methods the (R-W) model was restricted to the same spectral interval that McClatchey used, and a cooling rate computation was made for one of the cases given in McClatchey's paper; the results were sufficiently similar, so we did not compare McClatchey's results with any of the other models.

(M-S) MODEL

For the computation of infrared cooling due to water vapor the mean transmissivity (or mean absorptivity), which is weighted with respect to the temperature derivative of the black body emission, is defined for the entire

band as Yamamoto [25] suggested. The random model is used for the computation of mean transmissivity. The large temperature dependence of the mean absorptivity below 200° K. is considered for the flux computation by introducing the so-called emissivity at 220° K. The mean half width and mean line intensity are determined using the experiment of Howard et al. [6] and the theoretical computation of line intensity of Yamamoto. The continuum was treated as if it were a band with random model structure.

The absorptivity of the 15-micron band of carbon dioxide and that of the 9.6-micron band of ozone are determined using the results of laboratory measurement of absorptivity, which were carried out by Burch et al. [2] and Walshaw [24] under various pressures. See page 257 of Manabe and Wetherald [14] for the method of determining the absorption curve used for the computation. In order to estimate the temperature dependence of the absorptivity of the 15-micron band, the theoretical computation of the absorption by this band by Sasamori [21] is used. The temperature dependence of ozone absorption is neglected. The scaling approximation was used for incorporating the pressure effect.

Computation time for an 18-level (M-S) model is about 0.4 sec. on the UNIVAC 1108 computer, or about one-fourth the time of the (R-W) model.†

(PLASS) CO_2 MODEL AND (PLASS) O_3 MODEL

For the computation of infrared cooling due to the 15-micron band of carbon dioxide, the laboratory measurement of Cloud [3] is used. The band is subdivided into 1-micron intervals and the radiative flux divergence is computed for each interval. The effect of the temperature dependence of line intensity is taken into consideration. The two parameter-scaling approximation of pressure and optical thickness is used for treating the atmospheric inhomogenity.

For the computation of infrared cooling due to the 9.6-micron band of ozone, the results from the laboratory measurements of Summerfield‡ [23] are used. The effect of the temperature dependence of absorptivity is neglected.

(H-H) O_3 MODEL

The band model is not used. The Lorentz line shape is assumed. The smallest interval chosen (near the line center) is equal to the line width at 5-mb. pressure. The contribution of each subinterval to the infrared cooling is estimated. The treatment of the pressure effect is exact. The theoretical line strength of Kaplan, Migeotte, and Neven [8] is normalized upon Walshaw's [24] data, because their theory takes no account of severe Coriolis interaction.

(K) CO_2 MODEL

One of the most sophisticated numerical models has been proposed by Kaplan [9]. After dividing the absorption band into very narrow intervals of about 10/cm., the absorptivity is computed either by assuming a random model, or the Elsasser model and the multiplication properties for overlapped subband, whichever is appropriate. Pressure effects are included by the use of Curtis-Godson Approximation. The effect of temperature on the line intensity is incorporated exactly. It is probable that this model consumes 10–20 times as much computation time as (R-W) model. Therefore, this model is still not suitable for incorporation into the general circulation model.

3. COMPARISON OF RESULTS

(M-S) MODEL AND (R-W) MODEL

The vertical distributions of temperature, water vapor, and ozone, which are used for this comparison, are shown in figure 3. The exact values are given in table 1. For carbon dioxide a constant mixing ratio of 0.456 gm./kg. is used at all levels in the atmosphere. Figure 4 shows the cooling rate comparison for each of the absorbers and figure 5 shows the flux distribution when all three absorbers are present.

Water vapor—The agreement between the two results shown in figure 4 is excellent in the stratosphere and upper troposphere. There are some differences between the two results in the lower troposphere. This discrepancy is

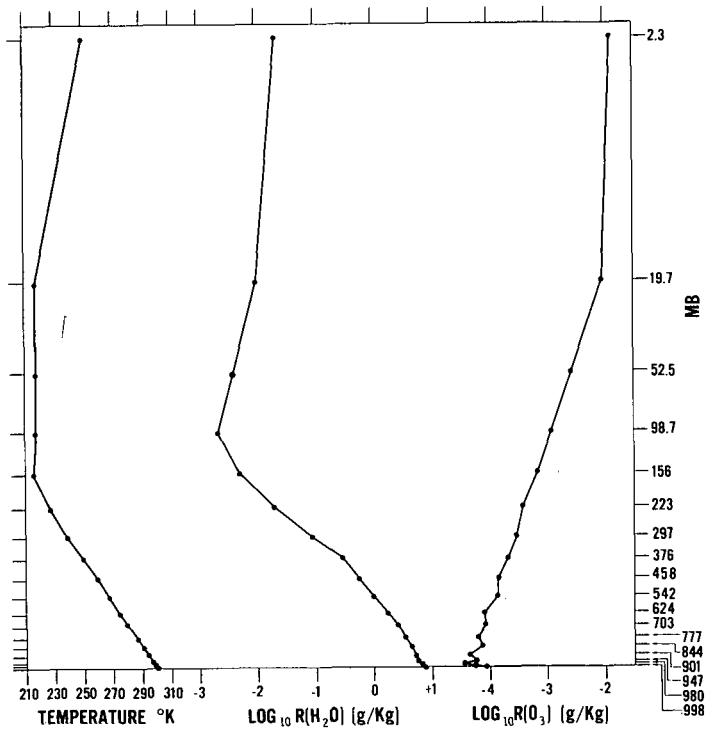

FIGURE 3.—Temperature, water vapor, and ozone distributions used for computations of figure 4.

†When the (M-S) model is used in the general circulation model [13], about 6 percent of the total computation time is used by the radiation program (assuming the long wave radiation computation is done four times per forecast day, which is sufficiently often, since it changes slowly with time).

‡The result of Summerfield [23] is quite different from that of Walshaw [24], which was obtained more recently.

TABLE 1.—*Values of temperature, water vapor, and ozone used for comparison of (M-S) model and (R-W) model*

Pressure (mb.)	Temperature (°K.)	Mixing Ratio (gm./kg.)	
		R (Water)	R (Ozone)
0.0000	251.3879	0.0000	0.000000
2.2719	251.3879	.0229	.012436
19.6759	218.1012	.0105	.009136
52.5120	218.5738	.0039	.002766
98.7226	218.0662	.0022	.001148
156.2500	215.9686	.0050	.000676
223.0367	226.7878	.0201	.000372
297.0250	239.2173	.0860	.000290
376.1574	250.0018	.2930	.000202
458.3762	259.4072	.5730	.000139
541.6238	267.6333	1.0400	.000139
623.8426	274.8176	1.7700	.000080
702.9750	281.0544	2.6400	.000085
776.9633	286.3196	3.4800	.000062
843.7500	290.8185	4.3700	.000071
901.2774	294.4844	5.2200	.000044
947.4880	297.3169	5.9700	.000058
980.3241	299.2888	6.5700	.000033
997.7281	300.3594	7.0000	.000094
1000.0000	300.3594	7.0000	.000094

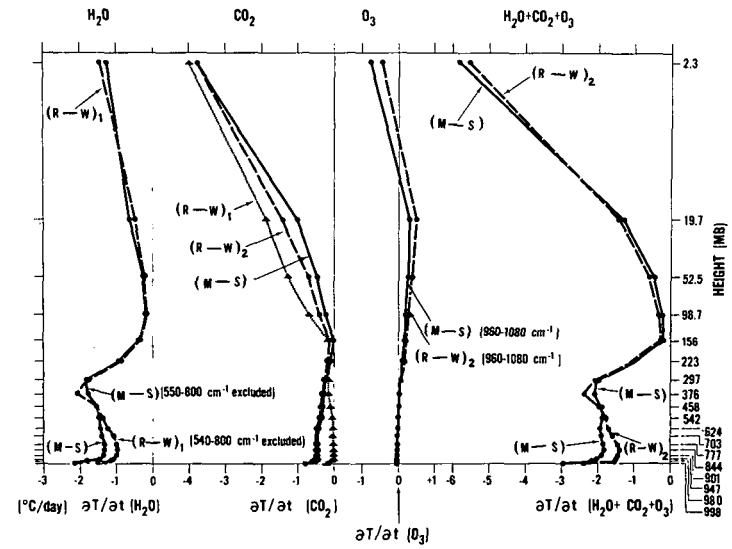

FIGURE 4.—Comparison of heating rates computed by the (M-S) and (R-W) models.

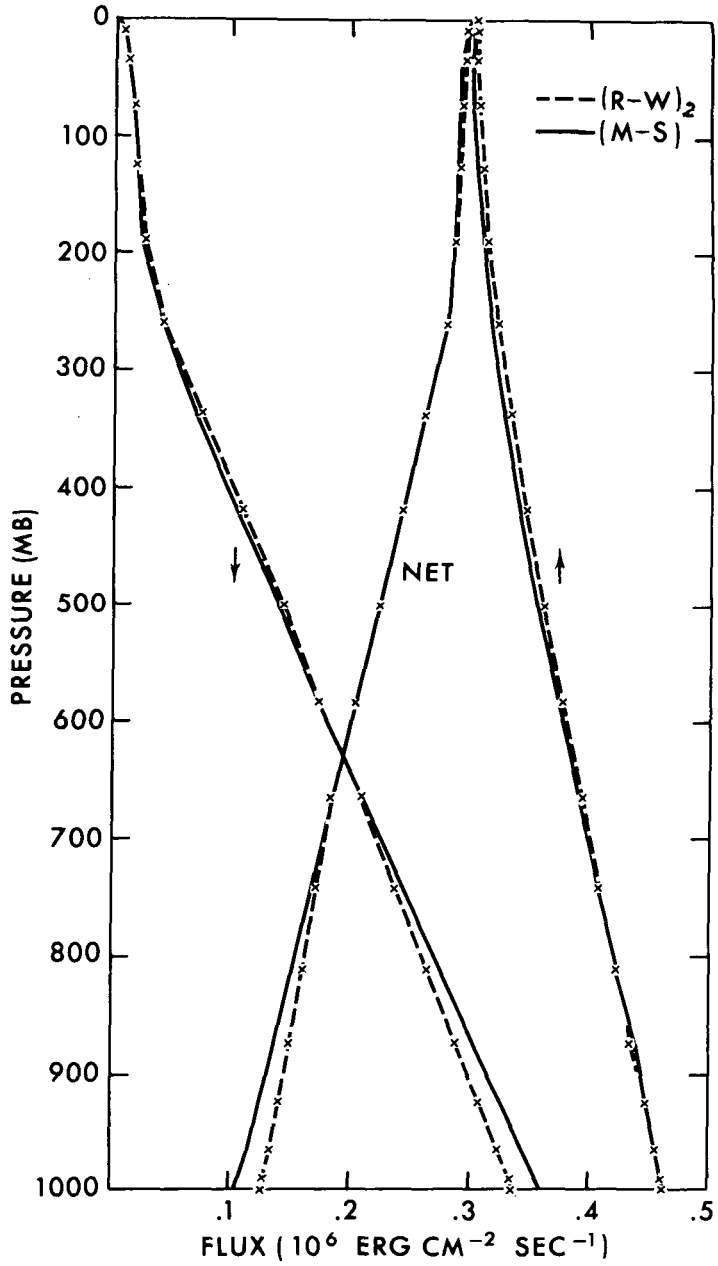

FIGURE 5.—Comparison of upward, downward, and net long wave radiation flux from (M-S) and $(R\text{-}W)_2$ models, with all three absorbers present.

partly caused by the different absorptivities used in the two models. These absorptivities are compared in figure 6; the solid curves are used in the (M-S) model and the dashed curves are from the (R-W) model. The absorptivities differ because mean half width and line intensity and the treatment of continuum are different. A comparison of the rotation band line intensities is given in figure 7. The (M-S) model uses the line intensities of Yamamoto [25], shown by the smooth curve, while the (R-W) model uses the line intensities of Benedict and Kaplan [1], the stepped curve. Figure 7 shows that the two intensities are significantly different. A series of test computations with the (R-W) model revealed that about 50 percent of the discrepancy in cooling rate in the lower troposphere (fig. 4) was due to these different line intensities. The remainder of the discrepancy is mostly due to the differences in the treatment of continuum and that of pressure effect.

Carbon dioxide—$(R\text{-}W)_1$ model yields practically no infrared cooling due to carbon dioxide in the troposphere (fig. 4). This unrealistic result is caused by the unrealistic absorptivity, which we have already discussed.

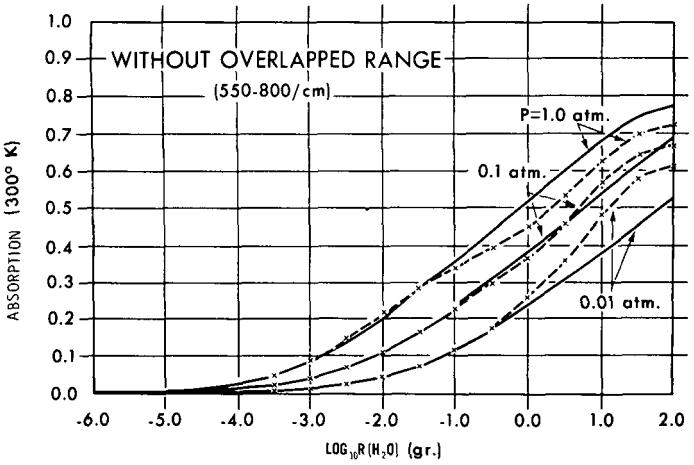

FIGURE 6.—Mean slab absorptivity of water vapor at temperature 300°K. Solid lines and dashed lines are obtained using the experimental results of Howard et al. [6] and the theoretical results of Benedict and Kaplan [1] respectively. The contribution from the wave number range 550–/cm. is not included for this computation.

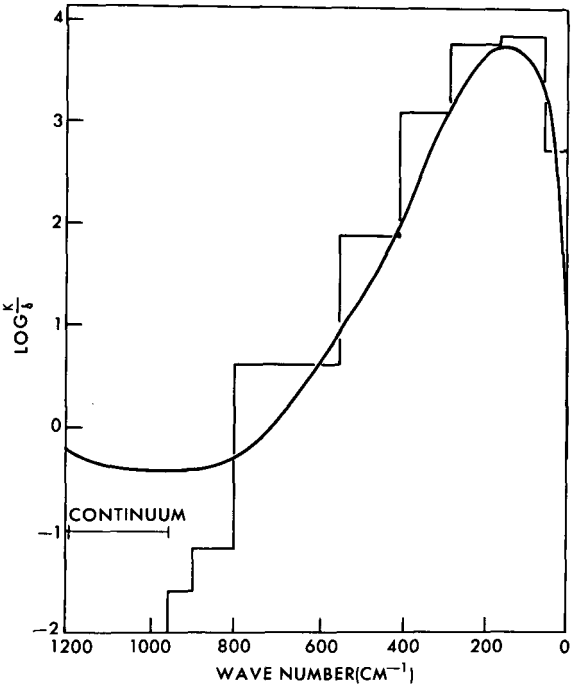

FIGURE 7.—Line intensities for the water vapor rotation band. Smooth curve due to Yamamoto [25], stepped curve computed from Benedict and Kaplan [1] data, for temperature 260°K.

The agreement between the results from the $(R\text{-}W)_2$ model and that from the (M-S) model is reasonably good.

Ozone—The agreement between the results from the $(R\text{-}W)_2$ model and those from the (M-S) model is fair (fig. 4). This difference is mainly caused by the difference between the Curtis approximation and the scaling approximation used for the (M-S) model. This was verified by substituting the scaling approximation for the Curtis

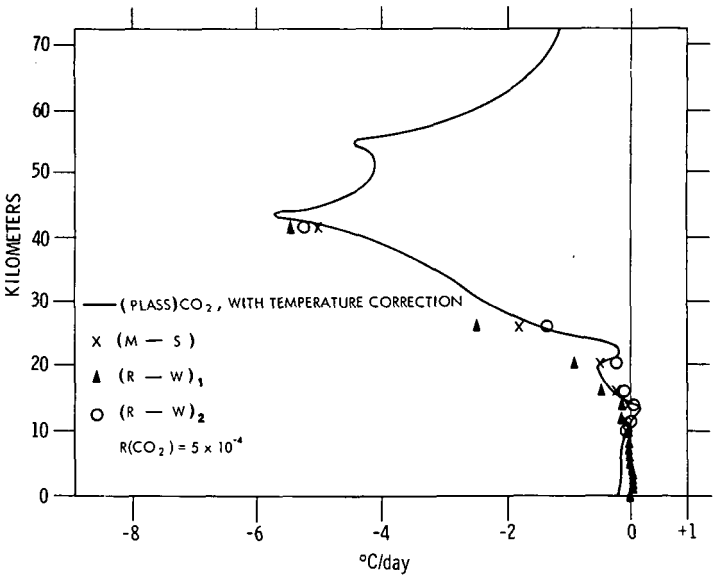

FIGURE 8.—Carbon dioxide heating rate of Plass [19] compared with other models. The (M-S) and $(R\text{-}W)_2$ results are identical with Plass in the lower 10 km., but are not plotted.

approximation in the (R-W) model. The scaling factor of (M-S) model is 0.3 for ozone. This resulted in a heating rate much closer to that of the (M-S) model.

Water vapor plus carbon dioxide plus ozone—The agreement is good except for the minor difference in cooling rate in the lower troposphere (fig. 4). This difference in cooling rate is consistent with the flux distribution of figure 5; net flux of the $(R\text{-}W)_2$ model is about 20 percent larger than that of the (M-S) model at the 1000-mb. level. The flux differences at high pressures are caused by the different water vapor absorptivities (fig. 6) used in the two models, as already discussed.

(PLASS) CO_2 MODEL AND OTHER MODELS

According to figure 8 the agreement among the results from (Plass) CO_2 model, from the (M-S) model, and from the $(R\text{-}W)_2$ model is excellent. The result from the $(R\text{-}W)_1$ model agrees with other results only at higher levels where the pressure is low and overlapping between lines is small.

(H-H) O_3 MODEL AND OTHER MODELS

Figure 9 shows that the agreement among the results of the (H-H) O_3 model and other models is fair. Again, the difference between the result from the (M-S) model and that of the $(R\text{-}W)_2$ model is mainly caused from the difference in the treatment of the pressure effect on the ozone absorption. It is interesting that the (M-S) model approximates the (H-H) model a little better than the $(R\text{-}W)_2$

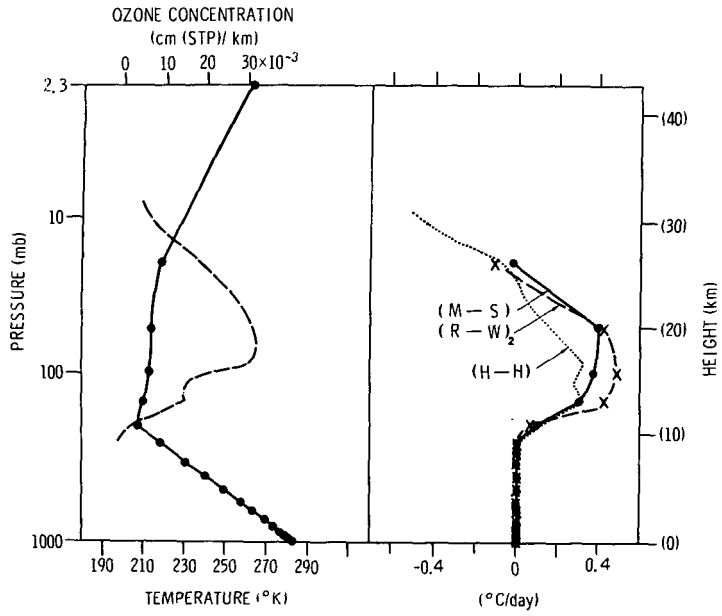

FIGURE 9.—Ozone heating rate of Hitchfeld and Houghton [5] compared with other models. In left portion, solid curve is temperature profile and dashed curve ozone distribution.

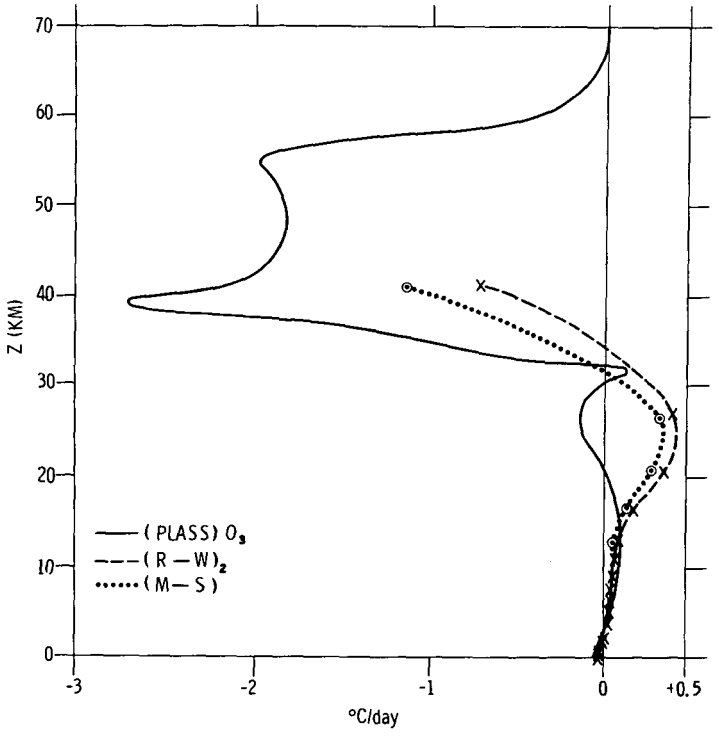

FIGURE 10.—Ozone heating rate of Plass [18] compared with other models. (M-S) and $(R\text{-}W)_2$ are identical in the lowest 10 km.

TABLE 2.—*Difference in net flux (erg cm.$^{-2}$sec.$^{-1}$)*

	Top	Bottom
$(R\text{-}W)_2$	3946	5200
(M-S)	3900	5300
(K)	3497	4889

model. Although it is probable that the scaling approximation is more accurate for this band than the Curtis-Godson approximation, we can not conclude so convincingly, because of the ambiguity involved in the determination of line intensity for (H-H) model.

(PLASS) O_3 MODEL AND OTHER MODELS

Figure 10 shows that the results obtained from the (M-S) and $(R\text{-}W)_2$ models are quite different from Plass' results. This is mainly due to the difference between the absorptivity of Summerfield [23] and that of Walshaw [24].

(K) CO_2 MODEL AND OTHER MODELS

Unfortunately, the example of the computation of temperature change, which is obtained by the (K) model, is not available to us. Using this model, Kaplan [10] estimated the dependence of net flux on the amount of carbon dioxide present in the atmosphere. In table 2, his results for a cloudless atmosphere, surface temperature 0°C., lapse rate 5.7°C./km., are compared to the changes in net flux obtained from the $(R\text{-}W)_2$ and (M-S) models. The values in table 2 are the difference in net flux at the top and bottom of the atmosphere when the carbon dioxide amount is changed from 130 cm. STP to 260 cm. STP. Though the dependence on carbon dioxide amount which is obtained by the (K) model is somewhat smaller than that obtained by the other two models, the agreement among the results is good.

4. CONCLUSION

The vertical distributions of the rate of temperature change due to the long wave radiation, which are obtained using the variety of methods, are compared with each other.

Generally speaking, the results from the Manabe-Strickler model agree reasonably well with those from the Rodgers and Walshaw model, or the Plass CO_2 model, despite the scaling approximation which is adopted for the (M-S) model.

There are some minor discrepancies among the results of the various authors, particularly among the computations of the effect of the 9.6-micron band of ozone.

In conclusion, the scheme of computing radiative transfer that is incorporated into the general circulation models of GFDL has comparable accuracy with other schemes despite various simplifications which are adopted for the model.

ACKNOWLEDGMENTS

The authors are very grateful for the encouragement of Dr. Joseph Smagorinsky throughout the course of this study. We appreciate the help of Mrs. Marylin Varnadore, Mrs. Clara Bunce and Mrs. Joyce Simpson in preparing the manuscript.

REFERENCES

1. W. S. Benedict and L. D. Kaplan, "Calculation of Line Width in H_2O-N_2 Collisions," *Journal of Chemical Physics*, Vol. 30, No. 2, 1959, pp. 388–399.
2. D. E. Burch, D. Gryvnak, and D. Williams, *Infrared Absorption by Carbon Dioxide*, Contract AF19(604)-2633, AFCRL-255, Ohio State University, Columbus, 1961.
3. W. H. Cloud, "The 15 Micron Band of CO_2 Broadened by Nitrogen and Helium," *Progress Report*, Contract-Nonr-248(01), Johns Hopkins University, Baltimore, Jan. 1952, 19 pp.
4. W. M. Elsasser, "Heat Transfer by Infrared Radiation in the Atmosphere," *Harvard Meteorological Studies*, No. 6, Harvard University Press, Cambridge, Mass., 1942, 107 pp.
5. W. Hitchfeld and J. T. Houghton, "Radiative Transfer in the Lower Stratosphere Due to the 9.6 Micron Band of Ozone," *Quarterly Journal of the Royal Meteorological Society*, Vol. 87, No. 374, Oct. 1961, pp. 562–577.
6. J. N. Howard, D. L. Burch, and D. Williams, "Near-Infrared Transmission Through Synthetic Atmospheres," *Geophysical Research Paper* No. 40, U.S. Air Force Cambridge Research Center, Nov. 1955, 244 pp.
7. B. G. Hunt and S. Manabe, "Experiments With a Stratospheric General Circulation Model: II. Large-Scale Diffusion of Tracers in the Stratosphere," *Monthly Weather Review*, Vol. 96, No. 8, Aug. 1968, pp. 503–539.
8. L. D. Kaplan, M. V. Migeotte, and L. Neven, "The 9.6 Micron Band of Telluric Ozone and Its Rotational Analysis," *Journal of Chemical Physics*, Vol. 24, No. 6, June 1956, pp. 1183–1186.
9. L. D. Kaplan, "A Method for Calculation of Infrared Flux for Use in Numerical Models of Atmospheric Motion," *The Atmosphere and the Sea in Motion—Scientific Contributions to the Rossby Memorial Volume*, The Rockefeller Institute Press, New York, 1959, pp. 170–177.
10. L. D. Kaplan, "The Influence of Carbon Dioxide Variations on the Atmospheric Heat Balance," *Tellus*, Vol. 12, No. 2, May 1960, pp. 204–208.
11. S. Manabe and F. Möller, "On the Radiative Equilibrium and Heat Balance of the Atmosphere," *Monthly Weather Review*, Vol. 89, No. 12, Dec. 1961, pp. 503–532.
12. S. Manabe and R. F. Strickler, "Thermal Equilibrium of the Atmosphere With a Convective Adjustment," *Journal of the Atmospheric Sciences*, Vol. 21, No. 4, July 1964, pp. 361–385.
13. S. Manabe, J. Smagorinsky, and R. F. Strickler, "Simulated-Climatology of a General Circulation Model With a Hydrologic Cycle," *Monthly Weather Review*, Vol. 93, No. 12, Dec. 1965, pp. 769–798.
14. S. Manabe and R. T. Wetherald, "Thermal Equilibrium of the Atmosphere With a Given Distribution of Relative Humidity," *Journal of the Atmospheric Sciences*, Vol. 24, No. 3, May 1967, pp. 241–259.
15. S. Manabe and B. G. Hunt, "Experiments With a Stratospheric General Circulation Model: I. Radiative and Dynamic Aspects," *Monthly Weather Review*, Vol. 96, No. 8, Aug. 1968, pp. 477–502.
16. R. A. McClatchey, "Infrared Heat Transfer by Atmosphere Water Vapor," *Journal of Applied Meteorology*, Vol. 3, No. 5, Oct. 1964, pp. 573–580.
17. F. Möller, "Das Strahlungs Diagram," *Reichsant für Wetterdienst (Luftwaffe)*, Berlin, 1943, 9 pp.
18. G. N. Plass, "The Influence of the 9.6 Micron Ozone Band on the Atmospheric Infra-Red Cooling Rate," *Quarterly Journal of the Royal Meteorological Society*, Vol. 82, No. 351, Jan. 1956, pp. 30–44.
19. G. N. Plass, "The Influence of the 15μ Carbon-Dioxide Band on the Atmospheric Infra-Red Cooling Rate," *Quarterly Journal of the Royal Meteorological Society*, Vol. 82, No. 353, July 1956, pp. 310–324.
20. C. D. Rodgers and C. D. Walshaw, "The Computation of Infra-Red Cooling Rate in Planetary Atmospheres," *Quarterly Journal of the Royal Meteorological Society*, Vol. 92, No. 391, Jan. 1966, pp. 67–92.
21. T. Sasamori, "The Temperature Effect of the Absorption of 15 Microns of Carbon-Dioxide Band," *Science Reports of the Tôhoku University*, Geophysics Ser. 5, Vol. 11, No. 3, Dec. 1959, pp. 149–161.
22. J. Smagorinsky, S. Manabe, and J. L. Holloway, Jr., "Numerical Results from a Nine-Level General Circulation Model of the Atmosphere," *Monthly Weather Review*, Vol. 93, No. 12, Dec. 1965, pp. 727–768.
23. M. Summerfield, "Pressure Dependence of the Absorption in the 9.6 Micron Band of Ozone," doctoral thesis, California Institute of Technology, Pasadena, 1941.
24. C. D. Walshaw, "Integrated Absorption by the 9.6μ Band of Ozone," *Quarterly Journal of the Royal Meteorological Society*, Vol. 83, No. 357, July 1957, pp. 315–321.
25. G. Yamamoto, "On a Radiation Chart," *Science Reports of the Tôhoku University*, Geophysics Ser. 5, Vol. 4, No. 1, June 1952, pp. 9–23.

[Received January 3, 1968; revised March 8, 1968]

PICTURE OF THE MONTH

A Catalina Eddy

JAY ROSENTHAL
Pacific Missile Range, Point Mugu, Calif.

Localized cyclonic eddies occur regularly in many parts of the world to the lee of protruding coastlines or topographic barriers. An example is the Catalina Eddy—so called because it frequently appears centered near the island of Santa Catalina off southern California (fig. 1). Among meteorologists of the area, there is little agreement as to what constitutes a Catalina Eddy other than a tendency towards cyclonic flow offshore (DeMarrais et al. [1]). Commonly attributed to orographic effects of the coastal mountains east of Point Conception, formation of the Eddy is a significant but largely unsolved forecast problem. It is generally reasoned that fields of convergence and vertical motion associated with eddy-producing situations cause a deepening of the marine layer with the end result being a substantial increase in extent, height, and daily duration of coastal stratus.

The development of a Catalina Eddy on May 27–29, 1968, is shown by a series of APT pictures recorded at the Pacific Missile Range Weather Center. An ESSA-6 picture on May 27 (fig. 2) shows coastal southern California

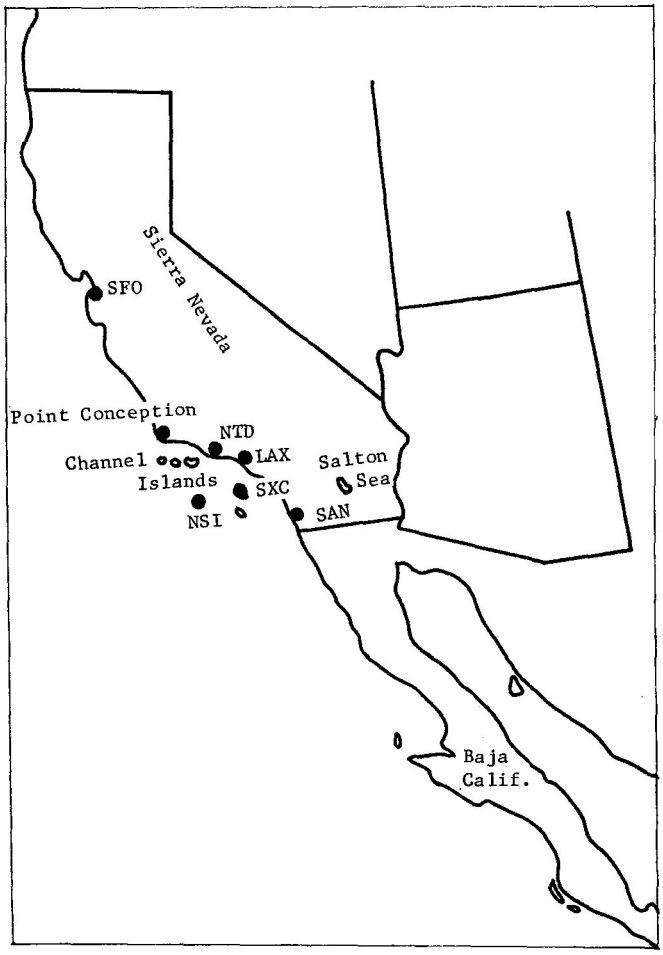

FIGURE 1.—Map of southwest United States and southern California coastal areas. Stations are identified as follows: SXC, Santa Catalina Island; NSI, San Nicolas Island; SAN, San Diego; LAX, Los Angeles International Airport; NTD, Point Mugu Naval Air Station; SFO, San Francisco.

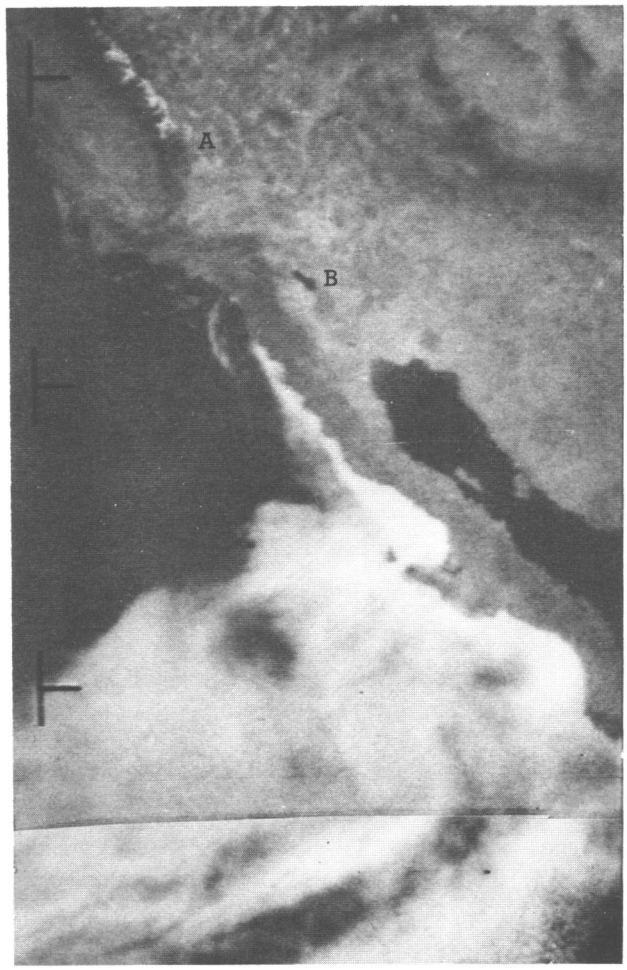

FIGURE 2.—ESSA-6, APT Pass 2494, 1728 GMT, May 27, 1968; (A) Sierra Nevada Mountains, (B) Salton Sea.

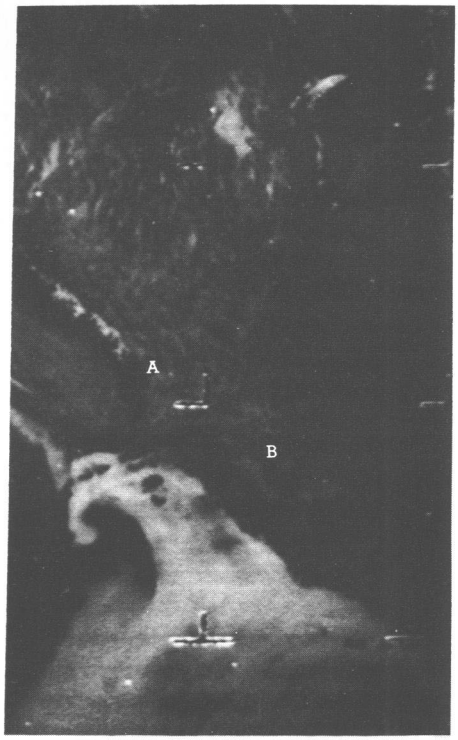

FIGURE 3.—ESSA-2, APT Pass 10401, 1523 GMT, May 28, 1968; (A) Sierra Nevada Mountains, (B) Salton Sea.

FIGURE 4.—ESSA-6, APT Pass 2507, 1821 GMT, May 28, 1968; (A) Sierra Nevada Mountains, (B) Salton Sea.

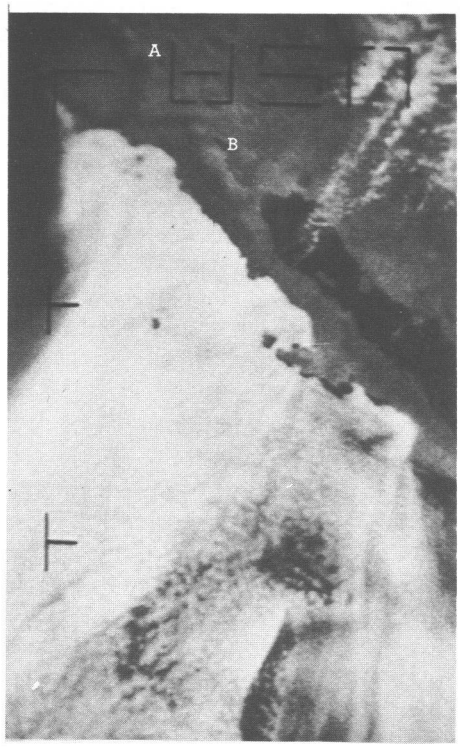

FIGURE 5.—ESSA-6, APT Pass 2519, 1716 GMT, May 29, 1968; (A) Sierra Nevada Mountains, (B) Salton Sea.

and adjacent waters free of cloud following a day with general offshore flow at the surface. Nearly all coastal stratus is restricted to Baja California. With normal inland penetration of hazy marine air prevented by the offshore flow, the coastline appears with remarkable clarity, as do interior landmarks such as mountains and the Salton Sea. Snow cover on the Sierra Nevada provides a fixed reference in this and succeeding pictures.

Even while clear conditions prevailed, evidence of eddy formation first appeared during the early morning hours of the 27th with cessation of much of the offshore flow and the onset of sporadic southeast winds at some coastal locations. Later in the day, more continuous southerly winds appeared at San Diego and at Los Angeles Basin stations as well, while winds at San Nicolas Island (elevation 571 ft.) turned to northeast. The first major effects of the Catalina Eddy were observed near midnight when brisk southeast winds were recorded at Point Mugu and fog and low stratus began to appear over much of the coast.

The invasion by stratus is shown vividly in the ESSA-2 picture taken the following morning (fig. 3). The prominent feature is a spiral formation whose outer boundary envelops the coastal area from the Mexican border to Point Conception. The inner boundary of this spiral between the cloudy air and the clear (presumably drier) air is sharply delineated. Depth of the cloud deck is generally shallow as several of the Channel Islands (whose maximum elevations range from 635 to 2,471 ft.) can be seen penetrating the stratus cover. Judging from the apparent progression of this spiral cloud pattern in the subsequent 3 hr. (fig. 4), the circulation is cyclonic in sense. In this latter picture, the pocket of clear air has now been cut off or isolated and is becoming mixed with cloudy air.

An ESSA-6 picture taken the next morning (fig. 5) reveals that stratus has engulfed the entire southern California coast and offshore waters, eliminating any trace of the pocket of clear air noticeable the previous day. The marine layer appears to have deepened considerably as only the highest portions of the islands are now visible through the cloud deck. Further evidence of a higher stratus deck is the substantially higher ceilings reported at coastal stations (Point Mugu ceilings were 1,500 ft. on the 29th as compared with zero-zero conditions at the time of stratus onset on the 28th). Even though pictorial evidence of continued cyclonic eddy circulation is not apparent, the deep marine layer and high stratus remain as testimony to the Catalina Eddy and its effects upon coastal southern California weather.

REFERENCE

1. G. A. DeMarrais, G. C. Holzworth, and C. R. Hosler, "Meteorological Summaries Pertinent to Atmospheric Transport and Dispersion Over Southern California," *Technical Paper* No. 54, U.S. Weather Bureau, Washington, D.C., 1965, 86 pp. (see p. 64).

[*Received August 7, 1968*]

WEATHER NOTE

HAILSTONES, STARFISH, AND DAGGERS—SPIKED HAIL FALLS IN OAK RIDGE, TENNESSEE

GARY A. BRIGGS

Air Resources Atmospheric Turbulence and Diffusion Laboratory, ESSA, Oak Ridge, Tenn.

There has never yet been a documented case of its "raining cats and dogs," but hailstones that recently fell at Oak Ridge exhibited a variety of unusual shapes, resembling starfish, turtles, anteaters, and even daggers. The striking feature was the long spikes that were generally coplanar and sometimes remarkably symmetrical. Photographs of selected hailstones are presented here, along with a description of the event.

The storm occurred on the morning of Mar. 12, 1968. Heavy precipitation including hail began abruptly at 0730 EST at a site 8 mi. south-southwest of us, and ended at 0750. Cloud to ground lightning was seen in the vicinity about this time. Spiked hailstones reached the ground at 0750 and fell about 7 min. at a recording station 3 mi. south-southwest of us. They were followed by 0.30 in. of rain in less than 5 min., and the rain ended there at 0805. Spiked hail began at 0800 here at ARATDL, located in the city of Oak Ridge. It was accompanied by a 1.6-mb. pressure jump and was followed by a downpour which ended at 0820. The wind was very light during the precipitation period.

When the rain ended, spiked hailstones, many undamaged, were lying about in the cushion of deep grass, and many people picked them up and stored them in their home refrigerators. Some of the stones lying in the grass retained their spikes over 40 min. after they fell (the air temperature was 12°C.). We photographed and collected a number of the stored stones 2 days after they fell, after receiving 17 responses to a request for them in the local newspaper. They were then forwarded to Dr. Charles Knight of the Ice Physics Laboratory at the National Center for Atmospheric Research for detailed analysis, which will be published at a later date.

Some idea of the range of shapes found in hailstones at one location can be inferred from figure 1. More extraordinary stones from the same location, 1 mi. southwest of here, are shown in figures 3 and 7. They were all collected by Bruce Johnson, a local 6th grader. Practically all of the stones had some spike development, the number of spikes ranging from one to six; most of the stones on the lawn at ARATDL had two, four, or six spikes. They were most often in a single plane, although a few had a single, short protrusion perpendicular to the dominant plane. The bodies of these stones were flattened, typically being 0.8 in. in diameter and 0.6 in. thick. They measured up to 2.2 in. overall. Somewhat larger and more grotesque stones with some non-coplanar spikes were found at the site 3 mi. south-southwest of Oak Ridge. Two of these are shown in figure 2.

Sketches of spiked hailstones have appeared from time to time in meteorological literature of the past century [1, 2]. However, some of the Oak Ridge hailstones are distinguished by an unusually high aspect ratio with the spike length exceeding the body diameter, as seen in figure 3. The spikes were up to 1 in. long. A few of the stones exhibited backswept spikes, as is seen in one of the stones in figure 3 and in figure 4. This phenomenon and the fact that few spikes were broken on impact suggest that many of these stones were aerodynamically stable and fell flat. A few others had spiralled arms, as was reported in [3]; these are shown in figure 5. Some of the stones also had lobes on the end of the spikes, as seen in figure 6. Perhaps the most striking stones were in the

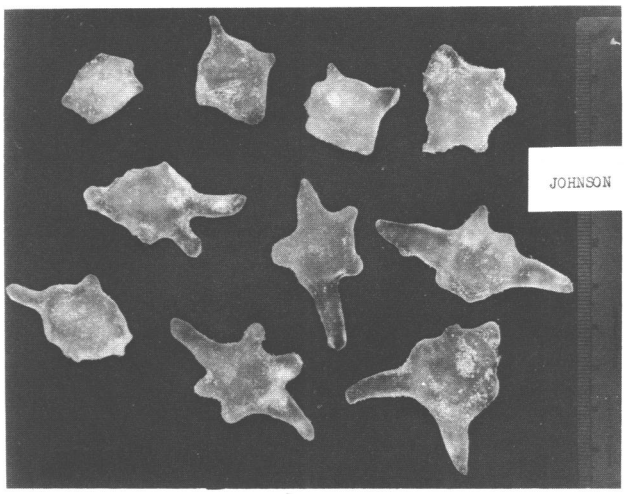

FIGURE 1.—Some forms of spiked hailstones, half original size, that fell in Oak Ridge.

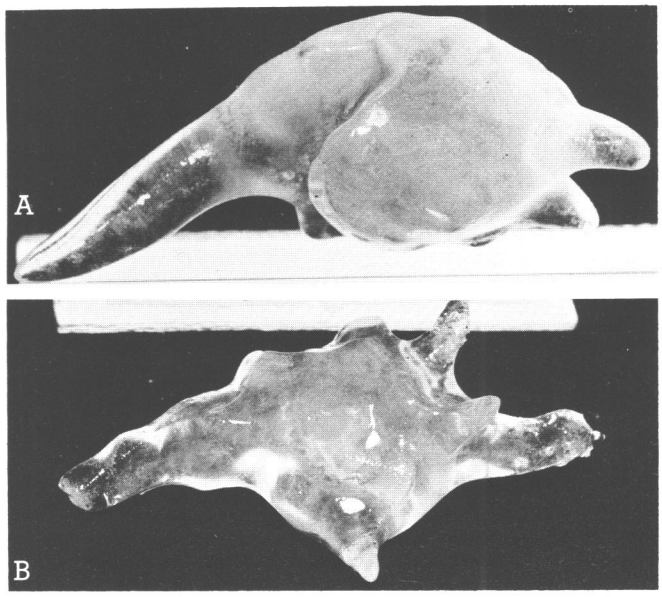

FIGURE 2.—Spiked hailstones (A, 1.6 and B, 1.1 times original size) found at the Y-12 plant, 3 mi. south-southwest of Oak Ridge.

FIGURE 3.—Long spikes 0.7 of original size.

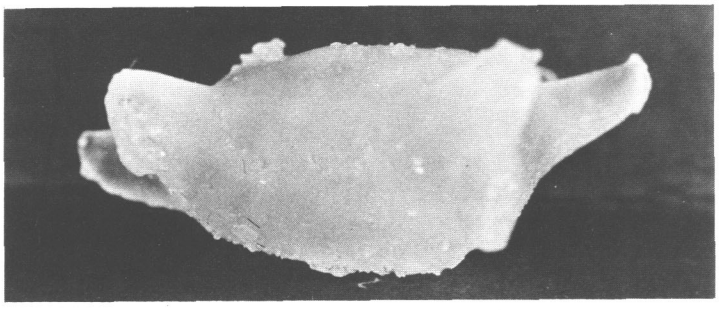

FIGURE 4.—Backswept spikes 2.8 times original size.

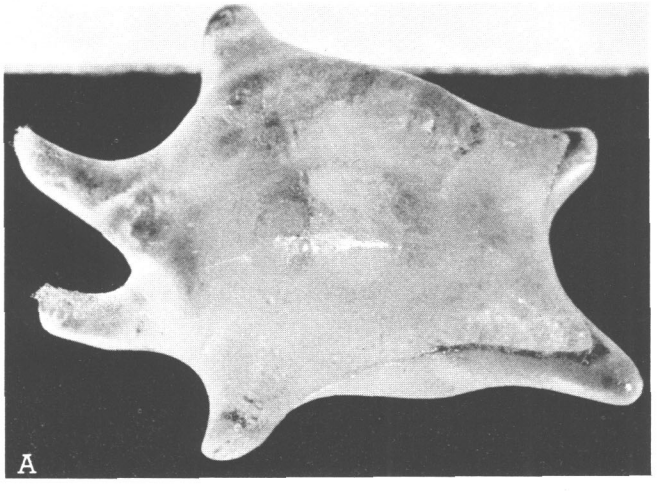

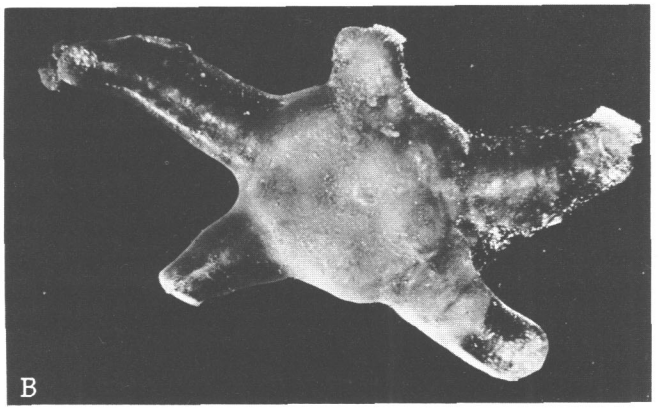

FIGURE 5.—Spiralled spikes (A, 2.9 and B, 1.7 times original size).

form of perfect crosses, or daggers, as illustrated in figure 7. Apparently one lobe broke off this specimen. About a half-dozen hailstones like this one were seen on the lawn here.

The storm appears to have been associated with a warm front, as was the storm which produced spiked

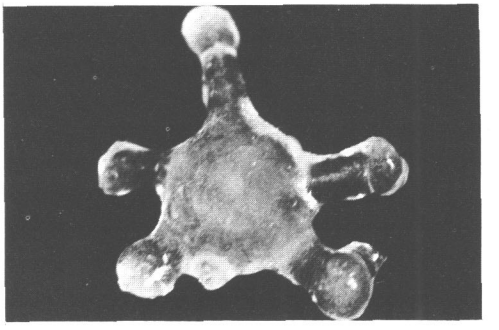

FIGURE 6.—Lobed spikes 1.3 times original size.

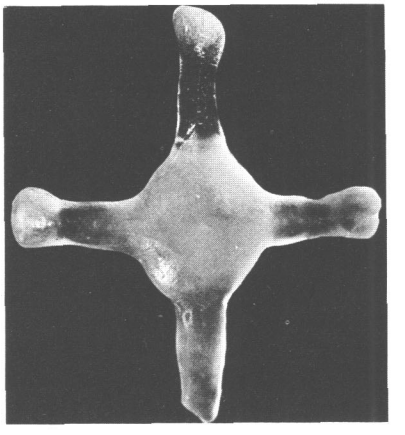

FIGURE 7.—Dagger-shaped hailstone 1.1 times original size.

hailstones at Bellport, Long Island [3]. The local meteorological records show evidence of a warm frontal passage at 1200 EST, followed by a cold frontal passage at 1500. The Nashville sounding for 0700, taken 130 mi. west of Oak Ridge, was unstable with respect to the wet adiabat up to 285 mb., with a very dry layer between 800 mb. and 500 mb. At that time, Nashville was also just north of the warm front, but was much closer to the center of the large low pressure area.

ACKNOWLEDGMENTS

Special thanks are extended to those area residents who braved the rain to collect these hailstones, especially to the following hailstone contributors: Bruce Johnson, Jamie Young, Rodney Bittner, Mrs. Grace Sweet, Mrs. Richard Lord, Mrs. Bettye Seivers, Mrs. Arthur Neely, and Mr. Karl Morgan. I am grateful to my colleagues, Mr. Walter Culkowski, Mr. Duane Turner, and Mr. George Gregory of the Air Resources Atmospheric Turbulence and Diffusion Laboratory, ESSA, who helped collect and photograph these stones, and to Dr. Charles Knight of NCAR for the photographs used in figures 1, 4, and 5.

REFERENCES

1. M. L. Rice and M. Rigby, "A Selective Annotated Bibliography on Hail," *Meteorological Abstracts and Bibliography*, Vol. 1, No. 4, American Meteorological Society, Apr. 1950, pp. 244–269.
2. E. Loomis, *Treatise on Meteorology*, Harper & Brothers, New York, 1868, 305 pp.
3. R. M. Brown, "Hail, Hail—A Case History," *Weatherwise*, Vol. 20, No. 1, Dec. 1967, pp. 254–258.

[*Received June 21, 1968*]